CHEMISTRY OF MATERIALS

Article

pubs.acs.org/cm

Theoretical Study of the Structural Evolution of a $Na_2FeMn(CN)_6$ Cathode upon Na Intercalation

Penghao Xiao,[†] Jie Song,[‡] Long Wang,[‡] John B. Goodenough,[‡] and Graeme Henkelman*[,†]

[†]Department of Chemistry and the Institute for Computational and Engineering Sciences and [‡]Texas Material Institute and Materials Science and Engineering Program, University of Texas at Austin, Austin, Texas 78712, United States

ABSTRACT: The Prussian Blue analog, $Na_xFeMn(CN)_6$, is a potential new cathode material for Na-ion batteries. During Na intercalation, the dehydrated material exhibits a monoclinic to rhombohedral phase transition, while the hydrated material remains in the monoclinic phase. With density functional theory calculations, the phase transition is explained in terms of a competition between Coulomb attraction, Pauli repulsion, and $d-\pi$ covalent bonding. The interstitial Na cations have a strong Coulomb attraction to the N anions in the host material, which tend to bend the Mn−N bonds and reduce the volume of the structure. The presence of lattice H_2O enhances the Pauli repulsion so that the volume reduction is suppressed. The calculated volume change, as it depends upon the presence of lattice H_2O, is consistent with experimental measurements. Additionally, a new $LiFeMn(CN)_6$ phase is predicted where MnN_6 octahedra decompose into LiN_4 and MnN_4 edge-sharing tetrahedra.

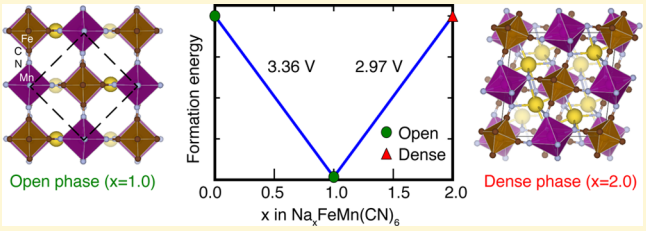

INTRODUCTION

Cathode materials for Li and Na batteries have attracted a great deal of interest for renewable energy applications.[1−3] They are also of interest scientifically, owing to the rich chemistry associated with ion intercalation processes. For example, intercalation of Li or Na ions can be coupled with displacive transformations of the host structures, resulting in complicated phase transitions and multiple voltage plateaus during electrochemical cycling.[4−6]

The Prussian blue analog (PBA), $Na_xFeMn(CN)_6$, has recently been discovered as a good cathode material for Na-ion batteries for its high gravimetric energy density and long cycle life. The actual structure of the active material, however, is under debate since different crystal structures have been reported due to small differences in the synthetic methodology.[7,8] Song et al. found that the amount of lattice H_2O plays an important role in the structural variation.[9] By completely dehydrating the material, two distinct phases are confirmed at different Na concentrations, a Na-poor monoclinic phase and a Na-rich rhombohedral phase. However, when fully hydrated, the structure of $Na_xFeMn(CN)_6{\cdot}2H_2O$ remains monoclinic over the entire range of Na concentration. These structural differences further affect the charge/discharge voltages. Understanding the atomic scale mechanism of these transformations is difficult solely from experiment. Even neutron diffraction, which is a powerful method for determining the structure of materials with light elements, has problems determining the Na occupation sites in the PBA and distinguishing atoms of Fe from Mn.

In this paper, theoretical studies are conducted to determine the structural changes in PBA during Na charge/discharge with consideration of the presence of lattice H_2O. Then, the underlying forces that influence the phase transitions are analyzed. In brief, during Na intercalation, the Coulomb attraction between Na and N anions tend to shrink the volume and stabilize the rhombohedral phase. The $d-\pi$ covalent bonding between Mn and N has the opposite effect and favors the linear structures found in the monoclinic phase with the larger volume. The introduction of H_2O into the lattice increases the Pauli repulsion, favoring the larger-volume monoclinic phase. The latter two forces together can eliminate the presence of the dense rhombohedral phase over the entire Na intercalation range. Finally, the correlation between the experimentally measured charging voltage and the host crystal structure is rationalized in this study with our computational model.

COMPUTATIONAL METHOD

Calculations based on density functional theory (DFT) were performed using the Vienna Ab-initio Simulation Package (VASP) with a plane-wave basis set and the projector augmented wave method to account for core electrons.[10−12] Two levels of theory were employed for the exchange correlation energy. First the general gradient approximation having the PW91 functional with a Hubbard on-site U term (GGA+U) on the transition metal d orbitals was used for structural optimization.[13,14] The DFT+U method is necessary to avoid artificial delocalization of electronic states, such as 3d electrons on the metal centers, as a result of the self-interaction error that is present in pure DFT. Effective U values (U_{eff}) of 4.3 eV for Fe and 5.0 eV for Mn were taken from the literature, originally developed for olivine $LiFePO_4$ and $LiMnPO_4$.[15−17] Soft potentials for C and N were employed with an energy cutoff of 360 eV for the plane-wave basis set. No significant difference was found with tests using harder potentials

Received: March 26, 2015
Revised: May 1, 2015
Published: May 12, 2015

DOI: 10.1021/acs.chemmater.5b01132
Chem. Mater. 2015, 27, 3763−3768

Table 1. Spin States and Lattice Parameters of $FeMn(CN)_6$ Calculated Using Different Functionals

method	spin state	spin	lattice parameters (Å)	space group
GGA	Mn: t_{2g}^4; Fe: t_{2g}^5	3	$a = b = 7.06$, $c = 9.91$	$I4/mmm$
GGA+U	Mn: $t_{2g}^3e_g^1$; Fe: t_{2g}^5	5	$a = 7.08$, $b = 7.31$, $c = 10.69$	$Immm$
HSE06	Mn: $t_{2g}^3e_g^1$; Fe: t_{2g}^5	5	$a = 7.00$, $b = 7.22$, $c = 10.61$	$Immm$

with a higher cutoff. The lattice parameters and formation energies were refined with the HSE06 hybrid functional, which mixes 25% exact exchange into PBE, with a range separation parameter of 0.2 Å.[18] The energy cutoff for the HSE06 calculations was set to 520 eV. The Monkhorst–Pack method was used to sample the Brillouin-zone with a k-point mesh of 2 × 2 × 2 for both DFT+U and HSE06. The reason for repeating our calculations with HSE06 is that it is more generally applicable and accurate than GGA+U; it is also more expensive.[19] Here we find that GGA+U, with our values of U_{eff}, gives reliable geometries, but the calculated voltages for Na intercalation differ from experiment whereas those from HSE06 are in agreement.

In the electronic ground state of PBA, Mn is in a high-spin state and Fe is low-spin. These spin states are expected because the crystal field splittings of MnN_6 and MnN_4 are small, while that of FeC_6 is large. During desodiation, Fe^{2+} is oxidized to Fe^{3+} first, and then Mn^{2+} is oxidized. Note that in desodiated structures, both the $Fe^{3+}Mn^{3+}$ and $Fe^{2+}Mn^{4+}$ electronic states are local minima with GGA+U and HSE06, but the latter configuration is higher in energy. Ferromagnetic configurations are the most stable for all compounds.

THEORETICAL RESULTS

In this section, we first compare different functionals on a well-defined phase of PBA to show the necessity to go beyond the GGA functional. With the right tool (HSE06), we then explain the observed phase transition seen in experiment. The structural changes upon intercalation without H_2O are calculated, and then the effects of lattice H_2O on the stable structures and intercalation voltages are discussed.

Comparison of Exchange Correlation Functionals. The GGA, GGA+U, and HSE06 functionals are employed to optimize the structure of the fully charged material, $FeMn(CN)_6$. The ground state spin configurations and lattice parameters are listed in Table 1. The GGA+U and HSE06 calculations are in qualitative agreement with each other. Specifically, Mn^{3+} is in a high-spin state and Fe^{3+} is in a low-spin state. The high-spin Mn^{3+} shows a strong Jahn–Teller effect, which elongates the c axis. Using HSE06, the Mn–N bond length is 2.22 Å along the c direction, while it is only 1.96 Å in the ab plane. Both the magnetic moments and the Jahn–Teller distortion have been observed experimentally.[9] The pure GGA functional, however, predicts a qualitatively incorrect ground state with Mn^{3+} in a low-spin state due to a lack of on-site Coulomb repulsion. As a result, no elongation is present along the c axis, and the lattice parameter is underestimated by 7%. This error is significant in light of the fact that GGA typically overestimates lattice constants by an error within 3% of experiment.[20] Thus, for PBA, GGA is not accurate enough to capture the correct electronic structure. GGA+U is sufficient for geometry optimization but not accurate enough to model the phase diagram of PBA, as we will show in the following section.

Na Intercalation in Dry PBA. Structural optimization with GGA+U shows that without any Na present in the lattice, the framework structure is orthorhombic with $Immm$ symmetry. MnN_6 and FeC_6 octahedra arrange in an alternating framework similar to cubic NaCl. While Mn and Fe ions are difficult to distinguish from X-ray and neutron diffraction, structural optimization, based upon DFT calculations, shows that Mn is coordinated by N and Fe is surrounded by C atoms. Mn^{3+} exhibits a strong Jahn–Teller distortion causing an elongation of the c axis. The ∠Mn–N–C and ∠Fe–C–N bond angles are both 180° to maximize the d–π orbital overlap. Intercalated Na tries to distort the structure because Na^{δ_x+} has a Coulomb attraction with the negatively charged N^{δ_y-}. At low Na concentration, the attraction is not strong enough to twist the entire framework, and the structure remains cubic-like, with nearly straight bond angles and the open monoclinic structure. Upon intercalation, Na occupies a lattice site on the face of the cube formed by four Fe and four Mn, closely coordinated by four N ions. Perhaps surprisingly, Na does not occupy the body center site despite the fact that this site has the most space to accommodate intercalating ions. The body center site is unfavorable because it is far from the negatively charged sites in the host to which Na binding is preferred. The occupation site preference agrees with previous calculations on $Na_xFeFe(CN)_6$.[21] With increasing Na concentration, the electrostatic energy from the Na–N ionic bonds increases proportionally to the total binding energy. Finally, at high Na concentrations, a denser rhombohedral structure becomes more stable in which the Na ions are coordinated by six N. The higher N coordination number forms at the cost of distorting the ∠Mn–N–C angle from 180° to 139°. The structural evolution is a result of the competition between the Na–N Coulomb attraction and the tendency to maintain linear Mn–N–C bonding to maximize the orbital overlap between N-2p and Mn-3d orbitals.

To confirm the importance of the ionic Na–N interactions, a comparison calculation was made in which only electrons are added to the $FeMn(CN)_6$ framework without the companion Na^+ ions. In this case, only the monoclinic structure is stable; the rhombohedral phase is not even a local minimum for $(FeMn(CN)_6)^{2-}$.

Figure 2 illustrates the transformation between the monoclinic and rhombohedral phases when PBA is half-sodiated. First, Na diffuses from a site coordinated by four N between two Mn to a site coordinated by three N between Fe and Mn. Second, the FeC_6 and MnN_6 octahedra rotate to bring three more N into coordination with Na. The minimum energy path calculated from the solid-state nudged elastic band method reveals that while these two steps are actually coupled together to lower the barrier, the minimum energy path is qualitatively as illustrated in Figure 2.[22]

At an intermediate Na concentration, the simulation cell is not strictly either monoclinic or rhombohedral. However, the series of crystal structures present during intercalation can still be classified into two families closely related to these crystal systems. The monoclinic family is characterized by straighter ∠Mn–N–C bond angles and a larger cell volume; the rhombohedral family has significantly bent ∠Mn–N–C bonds and a smaller cell volume. To avoid the crystal symmetry nomenclature, we label the framework structures based on their densities instead. We label the former as the open phase and the latter the dense phase. At intermediate Na concentration, both phases are local minima, and the relative formation

DOI: 10.1021/acs.chemmater.5b01132
Chem. Mater. 2015, 27, 3763–3768

energies can be compared. The convex hull, calculated from GGA+U, is plotted in Figure 1. When the Na intercalation

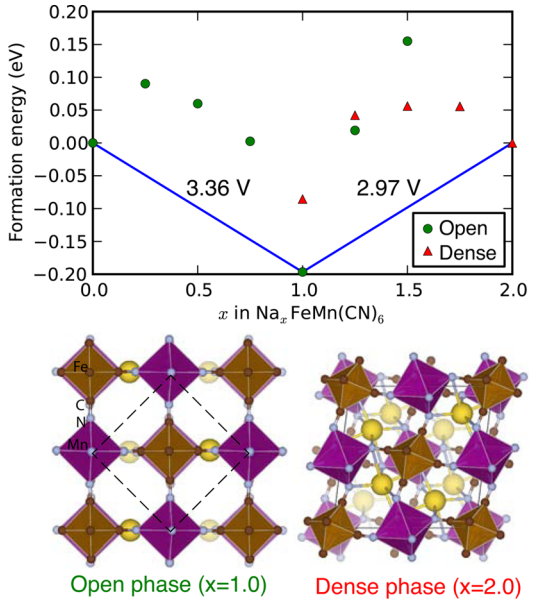

Figure 1. Convex hull and structures for the sodiation of PBA as calculated with GGA+U with values of U_{eff} = 4.3 for Fe and 5.0 eV for Mn. The formation energies are normalized per formula unit of $Na_xFeMn(CN)_6$. Coloring is as: brown polyhedra are Fe; purple are Mn; yellow spheres are Na; light blue are N; and deep brown are C.

fraction is more than 62.5% (x > 1.25), the dense phase becomes more stable than the open phase. Three structures lie on the hull: 0%, 50%, and 100% Na, resulting in two voltage plateaus for Na intercalation at 3.36 and 2.97 V.

In experiment only one plateau at 3.49 V is observed over the entire range of Na intercalation.[9] Since the Hubbard U_{eff} values were not tuned for this system, we compared these calculations to those of the more generally accurate HSE06 functional. The geometries essentially do not change from GGA+U to HSE06, except for a volume contraction of approximately 3%. The energetic ordering between the dense and open phases remains constant as well. In the HSE06-calculated convex hull plot of Figure 3, both half-sodiated structures are above the hull, which

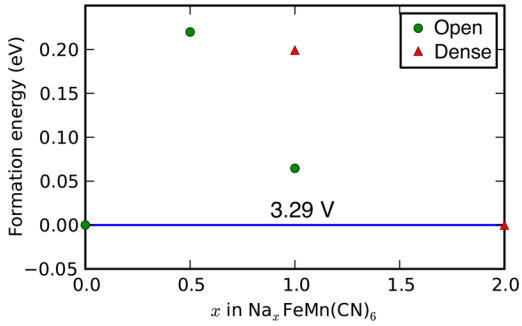

Figure 3. Convex hull for the sodiation of PBA as calculated using the HSE06 functional.

indicates a two phase equilibrium during charge/discharge at low current (near equilibrium), with a single voltage plateau at 3.29 V. The half filled structure may still be found in experiment, however, since it is only 0.06 eV per formula unit above the hull. Different U_{eff} values were tested, and it was found that U_{eff} = 2.0 eV for Fe and U_{eff} = 4.0 eV for Mn best match the HSE06 results. With these U_{eff} values, the half-filled structure is 0.12 eV above the hull, and the voltage plateau is at 3.25 V.

Na Intercalation in Hydrated PBA. With H_2O occupying sites in the lattice, the denser rhombohedral phase becomes less stable due to a stronger Pauli repulsion within the host structure. Water, in fact, has a similar effect as replacing Na with larger cations, such as has been observed with Rb.[23] In the presence of lattice H_2O, the Coulomb attraction has to compete with both the $d-\pi$ orbital overlap and the H_2O-enhanced Pauli repulsion in order to distort the structure and shrink the volume to form the denser rhombohedral structure.

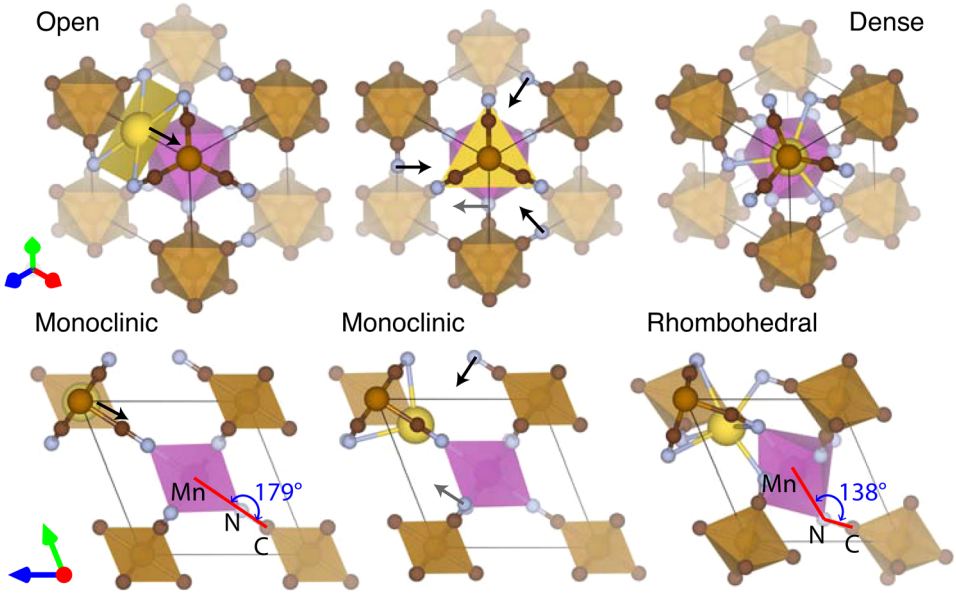

Figure 2. Transition from the monoclinic (open) phase to the rhombohedral (dense) phase. The middle structure is to illustrate the transition mechanism; it is not a saddle point.

DOI: 10.1021/acs.chemmater.5b01132
Chem. Mater. 2015, 27, 3763−3768

For the fully sodiated $Na_2FeMn(CN)_6{\cdot}xH_2O$, as the number x of H_2O molecules increases, the energy difference between the open and dense phases decreases until the open phase becomes energetically favorable for $x > 0.5$. The most stable fully sodiated and fully hydrated structures (with two H_2O per formula unit) from HSE06 are shown in Figure 4. Na−O−Na−

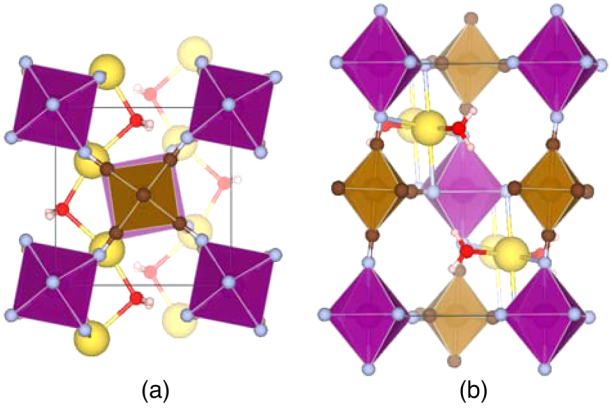

Figure 4. Structure of $Na_2FeMn(CN)_6{\cdot}2H_2O$: (a) top view and (b) side view.

O chains form inside the lattice as reported by Kareis et al.[23] A difference found in our calculations is that Na occupies an off-center site coordinated by four N atoms as in the open phase discussed in the previous section, not the cubic center site. The convex hull calculated from HSE06 with two H_2O per formula unit is plotted in Figure 5. H_2O brings the half-sodiated

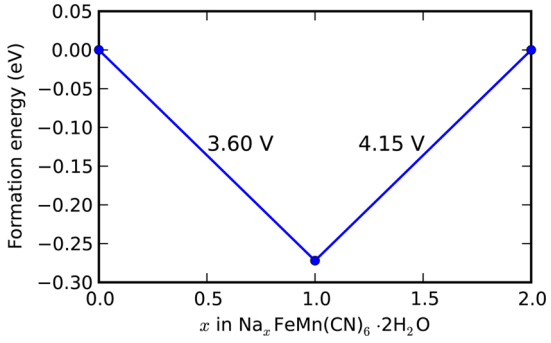

Figure 5. Convex hull for Na intercalation in hydrated PBA as calculated with the HSE06 functional.

structure down to the hull. In this structure, every other Na in the Na−O−Na−O chain is removed, and the remaining Na have the same arrangement as the left structure in Figure 1. The corresponding voltage plateaus are calculated to be 3.60 and 4.15 V. Although these values do not exactly match experiment, perhaps due to the uncertain quantity of water in the lattice, the trend is in qualitative agreement: lattice H_2O causes a phase transformation, two voltage plateaus, and an increase in the intercalation voltages. As Na is extracted, the binding energy of H_2O in the lattice becomes weaker, dropping from 0.8 eV to less than 0.1 eV as shown in Figure 6. This low H_2O binding energy in the fully charged state allows H_2O to escape in the deintercalation process, aided by the larger entropy in the electrolyte. After several cycles, the lattice H_2O concentration drops, which explains why the two plateaus merge and voltage decreases with cycling for cathodes containing lattice H_2O

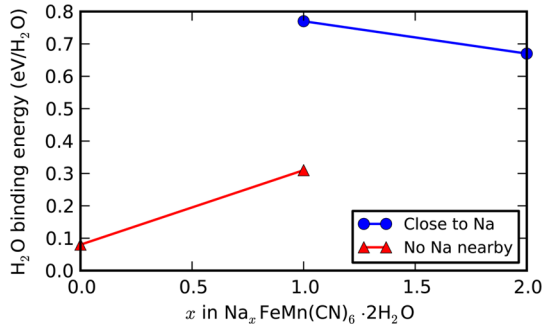

Figure 6. H_2O binding energy as a function of Na concentration, as calculated with the HSE06 functional.

initially. For more details about these experimental results, see Figure S5 in ref 9 and Figure 3(a) in ref 8.

The volume changes during Na intercalation are qualitatively different for the dry and hydrated PBA. Figure 7 shows a comparison of the calculated volume of the crystal and what is measured in experiment. This comparison can show which phase transitions the material undergoes during charging/discharging. From our HSE06 calculations, we can see that with or without H_2O the volume of the fully desodiated structure are essentially identical. When fully sodiated, however, the structure with H_2O expands in volume, while the one without H_2O reduces in volume. The experimental data show the same trends in volume changes between these four end points, as well as having quantitive agreement with the calculations. The volume changes demonstrate the strong interaction between the intercalated Na and the host framework, switching from Pauli repulsion to Coulomb attraction as H_2O is removed from the lattice.

Considering intermediate Na concentrations, there is a stable half-sodiated structure ($x = 1$) for hydrated PBA, with a volume that is larger than the end point structures ($x = 0, 2$). This increase in volume is seen both in experiment and theory. The dry PBA has a similar half-sodiated structure that is only slightly above the convex hull, shown as the left structure in Figure 1. If the battery was operated under equilibrium conditions, only the two structures on the hull should be visited, and no volume should be measured that is extremal to these the values of the end point structures. If the charge/discharge was somewhat out of equilibrium, however, the intermediate structure with a larger volume could be visited with a corresponding decrease of the first plateau voltage of 0.06 V. The experimental volume data indicate the presence of this half-sodiated structure. Note that the Na-poor phase line in Figure 7(b) is actually an interpolation of the fully desodiated $FeMn(CN)_6$ and half desodiated $NaFeMn(CN)_6$ structures. Interestingly, the charging voltage appears as a single plateau because the half-filled structure does not dominate the material and rather coexists with the other two stable structures. Another interesting fact worth mentioning is that the maximum volume change of this material is 27%, but its cyclability is excellent. Therefore, the volume change during charge/discharge does not necessarily result in bad cyclability.

The calculated lattice parameters and space groups of PBA are listed in Table 2 for reference. Some other 3*d* transition metals, including CuFe, FeFe, FeCo, FeNi, are also examined, but no qualitative difference is found for the structural evolution during charge; only small voltage shifts are found.

DOI: 10.1021/acs.chemmater.5b01132
Chem. Mater. 2015, 27, 3763−3768

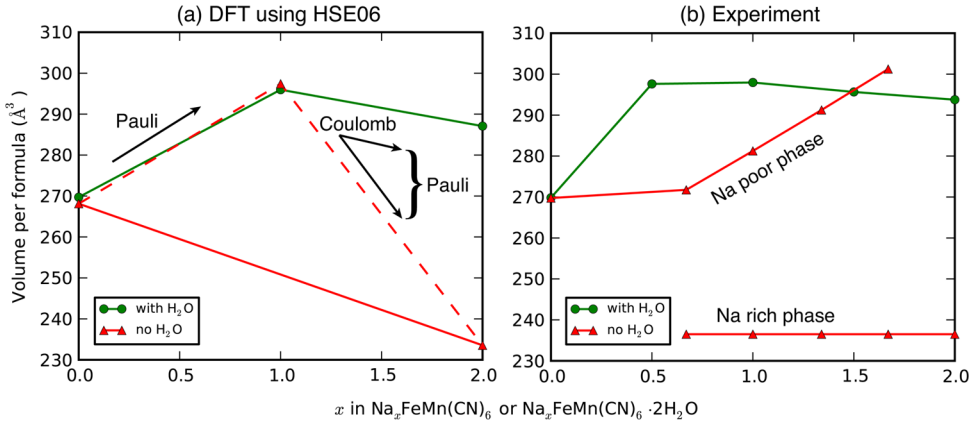

Figure 7. Volume change comparison between theory and experiment. (a) In the DFT results the solid lines represent the average volume of the formula unit in the crystal under equilibrium conditions. The dashed red line is out of equilibrium, in which the half-filled Na structure which is slightly above the convex hull is assumed to form. At low Na concentration, Pauli repulsion causes volume expansion during Na intercalation. After the host is half-filled, Coulomb attraction dominates and the volume shrinks. The difference between the red (dry) and green (hydrated) lines is due to the extra Pauli repulsion caused by H_2O molecules present in the lattice. (b) Experimentally, the volume of the Na poor and rich phases are determined separately; the value of x is simply an average of these two phases.

Table 2. Lattice Parameters (Å) and Space Groups

composition	space group	GGA+U	HSE06	experiment
$FeMn(CN)_6$	*Immm*	a = 7.09	a = 7.00	a = 7.15
		b = 7.31	b = 7.22	b = 7.15
		c = 10.69	c = 10.61	c = 10.54
$NaFeMn(CN)_6$	*Immm*	a = 7.19	a = 7.16	a = 7.54
		b = 7.97	b = 7.86	b = 7.54
		c = 10.67	c = 10.57	c = 10.66
$Na_2FeMn(CN)_6$	$R\bar{3}$	$a = b$ = 6.55	$a = b$ = 6.50	$a = b$ = 6.58
		c = 19.51	c = 19.13	c = 18.93
$FeMn(CN)_6 \cdot 2H_2O$	$P2_1/c$	a = 7.08	a = 7.01	a = 7.15
		b = 7.30	b = 7.21	b = 7.15
		c = 10.73	c = 10.67	c = 10.54
$NaFeMn(CN)_6 \cdot 2H_2O$	$P1$	a = 7.40	a = 7.37	a = 7.50
		b = 7.63	b = 7.57	b = 7.50
		c = 10.69	c = 10.62	c = 10.60
$Na_2FeMn(CN)_6 \cdot 2H_2O$	$P2_1/c$	a = 7.39	a = 7.36	a = 7.34
		b = 7.47	b = 7.42	b = 7.53
		c = 10.61	c = 10.53	c = 10.59

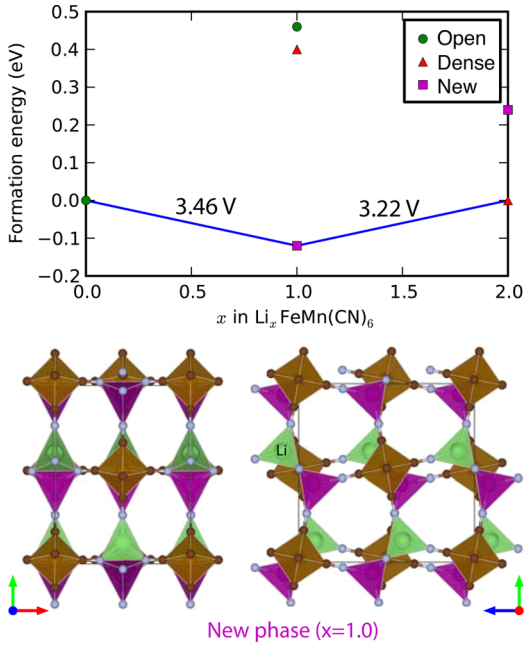

Figure 8. Calculated convex hull and a new half-filled structure of $Li_xFeMn(CN)_6$. Green tetrahedra are Li. The neighboring MnN_4 and LiN_4 are tetrahedra with shared edges.

Li Intercalation in PBA. Replacing Na by Li, the most stable structure at half-filling is different, as shown in Figure 8. The smaller size of Li means a shorter Pauli repulsion radius, which makes Li prefer to stay even closer to N as compared to Na. With increasing Li, some Mn−N bonds are even broken to form more Li−N bonds and lower the energy. In the half-filled structure, half of the ∠Mn−N−C angles are bent to 140° and half of them remain linear. Both Mn and Li are coordinated by four N, forming MnN_4 and LiN_4 tetrahedra paired by edge sharing. The new orthorhombic phase has a space group of $A2_1ma$ and a volume of 337.12 Å^3 per formula that is 10% larger than the half filled Na open phase. When the material is fully lithiated, the denser rhombohedral phase falls on the hull again, with a volume of 211.23 Å^3 per formula, which is then 13% smaller than the corresponding Na one.

CONCLUSION

In conclusion, the intercalation behavior of the PBA, $Na_xFeMn(CN)_6$, is understood by DFT calculations. The various phases observed are the results of three competing interactions: Na−N Coulomb attraction, $d-\pi$ orbital overlap, and Pauli repulsion. The Coulomb interaction tends to reduce the volume of the lattice, while the latter two resist the volume decrease. The introduction of lattice H_2O enhances the Pauli repulsion in the lattice and prevents the formation of the denser rhombohedral phase. Upon replacing Na with Li, the smaller ionic radius results in a weaker Pauli repulsion and leads to a completely new phase where Li is closely coordinated by N in a tetrahedron to minimize the Coulomb energy. An important conclusion from this work is that the ionic interactions between Li^+/Na^+ and the anions in the host structure need to be considered when designing new cathode materials. It is not always true that Li^+/Na^+ occupy the largest space in intercalation compounds. The space in the host material has

DOI: 10.1021/acs.chemmater.5b01132
Chem. Mater. 2015, 27, 3763−3768

to be at the right size to balance the Coulomb and Pauli interactions.

AUTHOR INFORMATION

Corresponding Author

*E-mail: henkelman@utexas.edu.

Notes

The authors declare no competing financial interest.

ACKNOWLEDGMENTS

This work is supported as part of the program "Understanding Charge Separation and Transfer at Interfaces in Energy Materials (EFRC:CST)" an Energy Frontier Research Center funded by the US Department of Energy, Office of Science, Office of Basic Energy Sciences under Award Number DE-SC0001091 and the Welch Foundation under Grants F-1841 (G.H.) and F-1066 (J.B.G.). Calculations were done with resources from the National Energy Research Scientific Computing Center and the Texas Advanced Computing Center.

REFERENCES

(1) Goodenough, J. B.; Park, K.-S. The Li-ion Rechargeable Battery: A Perspective. *J. Am. Chem. Soc.* **2013**, *135*, 1167−1176.

(2) Manthiram, A. Materials Challenges and Opportunities of Lithium Ion Batteries. *J. Phys. Chem. Lett.* **2011**, *2*, 176−184.

(3) Yabuuchi, N.; Kubota, K.; Dahbi, M.; Komaba, S. Research Development on Sodium-Ion Batteries. *Chem. Rev.* **2014**, *114*, 11636−11682.

(4) Delmas, C.; Maccario, M.; Croguennec, L.; Le Cras, F.; Weill, F. Lithium Deintercalation in $LiFePO_4$ Nanoparticles via a Domino-Cascade Model. *Nat. Mater.* **2008**, *7*, 665−671.

(5) Cogswell, D. A.; Bazant, M. Z. Coherency Strain and the Kinetics of Phase Separation in $LiFePO_4$ Nanoparticles. *ACS Nano* **2012**, *6*, 2215−2225.

(6) Liao, Y.; Park, K.-S.; Xiao, P.; Henkelman, G.; Li, W.; Goodenough, J. B. Sodium Intercalation Behavior of Layered Na_xNbS_2 ($0 \leq x \leq 1$). *Chem. Mater.* **2013**, *25*, 1699−1705.

(7) Lu, Y.; Wang, L.; Cheng, J.; Goodenough, J. B. Prussian Blue: A New Framework of Electrode Materials for Sodium Batteries. *Chem. Commun.* **2012**, *48*, 6544−6546.

(8) Wang, L.; Lu, Y.; Liu, J.; Xu, M.; Cheng, J.; Zhang, D.; Goodenough, J. B. A Superior Low-Cost Cathode for a Na-Ion Battery. *Angew. Chem., Int. Ed.* **2013**, *52*, 1964−1967.

(9) Song, J.; Wang, L.; Lu, Y.; Liu, J.; Guo, B.; Xiao, P.; Lee, J.-J.; Yang, X.-Q.; Henkelman, G.; Goodenough, J. B. Removal of Interstitial H_2O in Hexacyanometallates for a Superior Cathode of a Sodium-Ion Battery. *J. Am. Chem. Soc.* **2015**, *137*, 2658−2664.

(10) Kresse, G.; Hafner, J. Ab Initio Molecular Dynamics for Liquid Metals. *Phys. Rev. B* **1993**, *47*, R558−R561.

(11) Blöchl, P. E. Projector Augmented-Wave Method. *Phys. Rev. B* **1994**, *50*, 17953.

(12) Kresse, G.; Joubert, D. From Ultrasoft Pseudopotentials to the Projector Augmented Wave Method. *Phys. Rev. B* **1999**, *59*, 1758.

(13) Perdew, J. P.; Wang, Y. Accurate and Simple Analytic Representation of the Electron-Gas Correlation Energy. *Phys. Rev. B* **1992**, *45*, 13244−13249.

(14) Dudarev, S. L.; Botton, G. A.; Savrasov, S. Y.; Humphreys, C. J.; Sutton, A. Electron-Energy-Loss Spectra and the Structural Stability of Nickel Oxide: An LSDA+U Study. *Phys. Rev. B* **1998**, *57*, 1505−1509.

(15) Zhou, F.; Cococcioni, M.; Marianetti, C. A.; Morgan, D.; Ceder, G. First-Principles Prediction of Redox Potentials in Transition-Metal Compounds with LDA+U. *Phys. Rev. B* **2004**, *70*, 235121.

(16) Hinuma, Y.; Meng, Y. S.; Kang, K.; Ceder, G. Phase Transitions in the $LiNi0.5Mn0.5O_2$ System with Temperature. *Chem. Mater.* **2007**, *19*, 1790−1800.

(17) Chevrier, V. L.; Ong, S. P.; Armiento, R.; Chan, M. K. Y.; Ceder, G. Hybrid Density Functional Calculations of Redox Potentials and Formation Energies of Transition Metal Compounds. *Phys. Rev. B* **2010**, *82*, 075122.

(18) Heyd, J.; Scuseria, G. E.; Ernzerhof, M. Erratum: "Hybrid Functionals Based on a Screened Coulomb Potential". *J. Chem. Phys.* **2006**, *124*, 219906.

(19) Marsman, M.; Paier, J.; Stroppa, A.; Kresse, G. Hybrid Functionals Applied to Extended Systems. *J. Phys.: Condens. Matter* **2008**, *2222*, 064201.

(20) Haas, P.; Tran, F.; Blaha, P. Calculation of the Lattice Constant of Solids with Semilocal Functionals. *Phys. Rev. B* **2009**, *79*, 085104.

(21) Ling, C.; Chen, J.; Mizuno, F. First-Principles Study of Alkali and Alkaline Earth Ion Intercalation in Iron Hexacyanoferrate: The Important Role of Ionic Radius. *J. Phys. Chem. C* **2013**, *117*, 21158−21165.

(22) Sheppard, D.; Xiao, P.; Chemelewski, W.; Johnson, D. D.; Henkelman, G. A Generalized Solid-State Nudged Elastic Band Method. *J. Chem. Phys.* **2012**, *136*, 074103.

(23) Kareis, C. M.; Lapidus, S. H.; Her, J.-H.; Stephens, P. W.; Miller, J. S. Non-Prussian Blue Structures and Magnetic Ordering of $Na_2MnII[MnII(CN)_6]$ and $Na_2MnII[MnII(CN)_6]\cdot 2H_2O$. *J. Am. Chem. Soc.* **2012**, *134*, 2246−2254.

DOI: 10.1021/acs.chemmater.5b01132
Chem. Mater. 2015, 27, 3763−3768